DOI: 10.5604/01.3001.0054.1593
Volume 120 • Issue 2 • October 2023
Journal of Achievements in Materials and Manufacturing Engineering
International Scientific Journal published monthly by the World Academy of Materials and Manufacturing Engineering

Bending behaviour of a topologically optimised ABS mesostructures 3D printed by the FDM process: numerical and experimental study

I. Antar [a,*], M. Othmani [b], K. Zarbane [a], M. El Oumami [a], Z. Beidouri [a]
[a] Laboratory of Advanced Research on Industrial and Logistic Engineering, National Higher School of Electricity and Mechanics, Hassan II University of Casablanca, Casablanca, Morocco
[b] Laboratory of Mechanics Engineering and Innovation, National Higher School of Electricity and Mechanics, Hassan II University of Casablanca, Casablanca, Morocco
* Corresponding e-mail address: intissar.antar@ensem.ac.ma
ORCID identifier: https://orcid.org/0000-0002-6906-7030 (I.A.)

ABSTRACT

Purpose: This paper is intended to investigate numerically and experimentally the influence of raster angle on the structural performance of an optimised printed structure.

Design/methodology/approach: The topology optimisation (TO) problem for compliance minimisation using Solid Isotropic Material with Penalization (SIMP) method has been solved with a Messerschmitt-Bolkow-Blohm (MBB) beam under three-point bending, then the resulting optimal design was additively manufactured using Fused Filament Fabrication (FFF) with varying raster angle. The mechanical behaviour of these geometries was investigated and compared. A numerical approach has been developed through a script in Python based on the G-code file and integrated into an ABAQUS to create a virtual sample identical to the physical specimen. The numerical results were coupled with an experimental investigation.

Findings: The investigation presented in this work showed that the choice of raster significantly affects on the mechanical performance of the printed optimised structures. Indeed, the optimised structure printed with a 90° raster angle has the highest performance in contrast to 45° and 0°, while the optimised structure printed at a 45° raster angle has an average performance. The experimental test validated the numerical data with an error of approximately 1.09%. Our numerical results are in good conformity with the experimental outcomes.

Research limitations/implications: In this research, we studied the impact of three raster angles (90°, 45° and 0°) on the mechanical behaviour of a FFF optimised part. The subsequent study will focus on the other print parameters, including the other raster angles.

Practical implications: The analysis presented in this paper can be used for manufacturing a FFF optimised structure.

Originality/value: This paper evaluates the effect of raster angle in printed optimised structures using a novel numerical approach. The presented results will establish a reference that many researchers can gear to develop the fabrication of TO structures by incorporating printing parameters.

Keywords: FFF, Raster angle, Topology optimisation, SIMP, Mechanical behaviour

Reference to this paper should be given in the following way:
I. Antar, M. Othmani, K. Zarbane, M. El Oumami, Z. Beidouri, Bending behaviour of a topologically optimised ABS mesostructures 3D printed by the FDM process: numerical and experimental study, Journal of Achievements in Materials and Manufacturing Engineering 120/2 (2023) 66-74. DOI: https://doi.org/10.5604/01.3001.0054.1593

1. Introduction

In recent years, topology optimisation (TO) has been widely used in many industrial applications, such as aerospace, automotive, and architecture, to improve the efficiency of a product and reduce manufacturing costs. It seeks to fund an optimal structure through the distribution of the material in the design space, considering all predefined constraints and boundary conditions [1]. Numerous methods have been presented and developed for topology optimisation, including the SIMP, homogenisation [2,3], evolutionary structural optimisation, ESO, and level set methods. Fortunately, with the advance in additive manufacturing (AM), intricate structures can be produced layer-by-layer using various printing processes such as Selective Laser Sintering (SLS), Fused Filament Fabrication (FFF) and selective laser melting (SLM). The performance of printed parts, especially by FFF, is investigated by many authors, such as Abdeddine et al. [4], experimentally, according to the type of boundary conditions, the effect of large vibration. Costa et al. [5] examined, through the tensile test, the effect of envelope temperature, extrusion temperature, forced cooling and extrusion rate. Likewise, Aboma Wagari Gebisa et al. [6] studied the impact of five parameters: air gap, raster width, raster angle, contour number and contour width; their investigation has shown that the raster angle is the one parameter that significantly influenced the tensile properties. Therefore, combining the two fields allows designers to produce a lightweight structure with high performance in the shortest time and lowest cost. Hence, the optimised structure performance of AM processes can be impacted by different process printing parameters, which several researchers report. For instance, Kandemir et al. [7] proposed a novel approach for intermediate densities as a variable thickness and studied the mechanical properties of the printed models using two different materials; their approach increases the manufacturability and the mechanical properties of the printed models due to the continuity of the layers. Garcia et al. [8] have studied the influence of printing parameters on the stiffness/weight (mass) ratio of the models according to a three-point bending test. Their results showed that the part manufactured by Polyjet gives better accurate geometry than ABS-M30. Mohan et al. [9] have proposed a new design of an optimal geometry by ensuring the minimum FR with material continuity for manufacturing feasibility of AM while maintaining the same structural strength; they concluded that the structural performance of the AMTO geometry is lower compared to the conventional TO geometry. The effect of printing parameters on mechanical behaviour was also studied by Hmeidat et al. [10], for which the rectilinear and concentric infill patterns have been investigated numerically and experimentally. Their study has been shown that the optimised structures printed by rectilinear improve the mechanical performance. Many researchers have also studied lattice or cellular structures; for example, Rashid et al. [11] have studied the bending behaviour of the optimised lattice and solid beams.

This paper aims to investigate numerically and experimentally the influence of various raster angles on the optimised structure's structural performance through the three-point bending test.

The manuscript is structured as follows: Section 2 presents topology optimisation for minimising compliance used to determine the optimal structure applied on a Messerschmitt-Bolkow-Blohm (MBB) beam. Section 3 outlines the numerical approach to create the digital three-point bending test. Section 4 presents the experimental set-up of the bending test for the physical test specimens. Section 5 reports the results and discussion of the two procedures. Section 6 presents the conclusion of the paper.

2. Topology optimisation using the SIMP method for minimising compliance

Solid Isotropic Material with Penalization (SIMP) is the most used topology optimisation method. It is dependent on the relative densities. It aims to find an optimal distribution of material in the design domain [12], where the density of material varies between 0 and 1, where 0 represents the redundant material and 1 the solid material. The topology optimisation problem was solved for a minimisation of compliance subject to volume constraints.

$$Minimize: C(\rho) = \{F\}^t\{U\} = \sum_{e=1}^{N}(\rho_e)^P\{u_e\}^T[K_e]\{u_e\} \quad (1)$$

$$\text{s.t.} \begin{cases} \frac{V(\rho)}{V_0} = V_f \\ [K]\{u\} = \{F\} \\ 0 < \rho_{min} \leq \rho_e \leq 1 \end{cases} \quad (2)$$

where U and F are the global displacement and force vector, K is the global stiffness matrix, u_e and K_e are the element displacement vector and stiffness matrix, respectively. ρ_{min} is a vector of minimum relative densities, which is set to ρ_{min} = 0.001. N is the number of elements used to discretise the design domain; ρ is the penalisation power. This parameter penalises intermediate densities. $V(\rho)$ and V_0 is the material volume and design domain volume. V_f prescribes the volume fraction [13].

In the framework of this optimisation, Messerschmitt-Bolkow-Blohm (MBB) beam benchmark topology optimisation problem was optimised under a three-point bending test according to ISO 178, as is shown in Figure 1. using ABAQUS 2022 with dimensions of 80 mm x 10 mm x 4 mm. The load applied to the centre of the top edge has been set at 6 N, and the distance between the support span is 64 mm. The MBB beam was discretised by 25552 elements for linear hexahedral elements C3D8R used in mesh type. The required volume fraction was defined as follows: V_f = 0.3 and ρ = 3 for the SIMP factor. The filter radius is set to 0.6 mm. The problem is solved by the Optimality Criteria (OC).

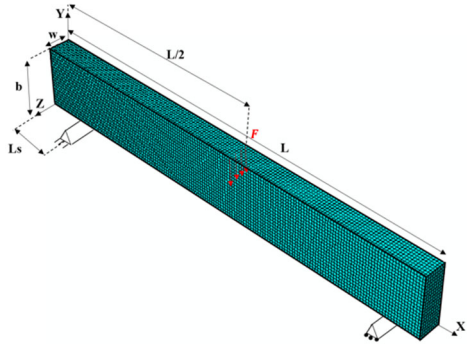

Fig. 1. Mesh and its typical size

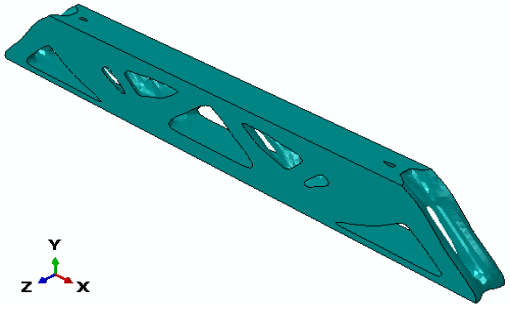

Fig. 2. Topology design of MBB beam

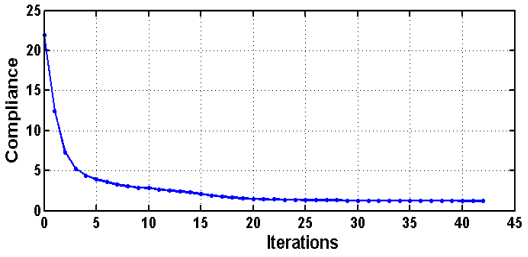

Fig. 3. Evolution history of the objective function

The optimisation process needed 42 iterations to achieve the optimal design presented in Figure 2. The convergence history for the MBB beam is given in Figure 3. The minimum compliance obtained for 30% of the preserved volume is 1.23 N.m.

3. Implementation of the numerical approach

In order to study the mechanical behaviour of the FFF printed parts, a numerical approach has been developed and presented. This approach enables a digitally optimised design similar to a printed shape. A Python script is developed in which all printing parameters are considered. This code runs in ABAQUS 2022 (Dassault Systems) to execute the G-code extracted from 'Slic3r', then draws the tool path and the raster section [14].

3.1. Configuration of the digital models

The virtual optimised model is obtained in several steps summarised in Figure .4. Initially, the CAD model of the optimised MBB beam mentioned above is saved in Stereo Lithography (STL) format. Then, its G-code file, which contains the commands that instruct the machine to deposit

Table 1.
Printing setting of the digital models

Parameters	Values
Layer thickness	0.4 mm
Raster angle	90°/45°/O°
Raster width	0.8
Overlap	5%
Infill pattern	Aligned rectilinear
First-layer printing speed	30 mm/s
Print speed of other layers	60mm/s
Number of perimeters	1
Bed temperature	100°
Nozzle temperature	240°C

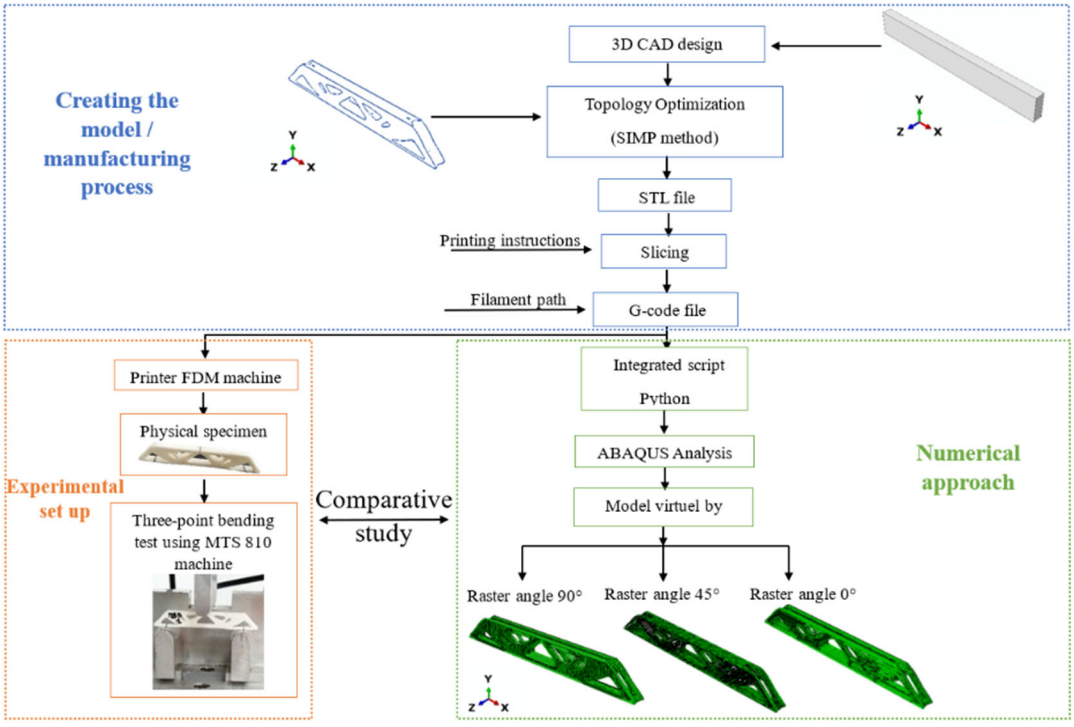

Fig. 4. Flowchart of the proposed approach

the filament, layer by layer, to construct an accurate geometric part, was extracted from "Slic3r" in order to reproduce the optimised structure considering the printing and filament settings stated in Table 1.

Secondly, then, a script in "Python" based on the G-code file has been developed and integrated into the "ABAQUS 2022." At the end of the script generation, the digital model was obtained with three raster angles.

3.2. Analysis

Once the generation of digital models is completed, the elastic constants of ABS are introduced [14]. Material is assumed to be homogeneous and isotropic in the analysis. Independent instance type is selected in the 'Assembly' module, and tie-type interaction contact is created between the contour and infill aiming to stick the filament between them to determine which part of the surface of the model comes into contact during the deformation [15].

The digital models have submitted similar boundary conditions to the previously optimised MBB beam. Linear 3D tetrahedral elements C3D4 (4 nodes linear tetrahedron) are used for meshing the virtual models. The boundary conditions and the mesh of the virtual models are shown in Figure 5.

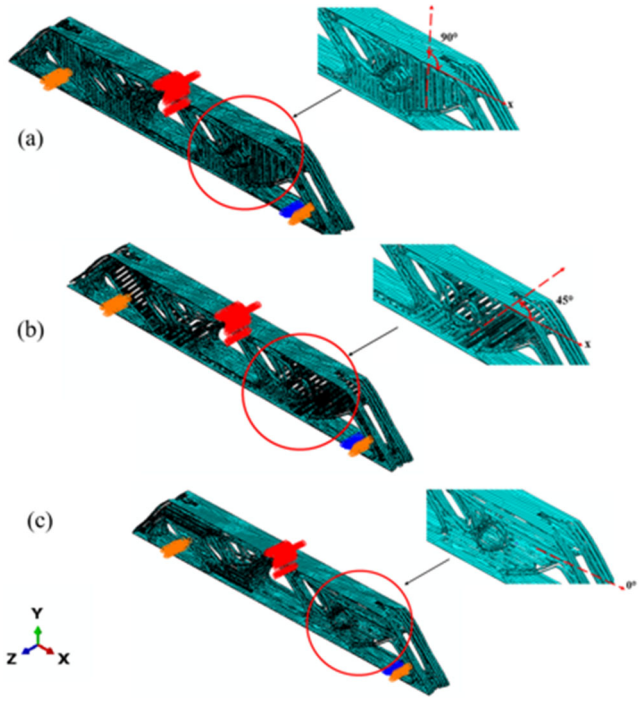

Fig. 5. Tetrahedral mesh and BC of the digital models for (a) 90°, (b) 45° and (c) 0° raster angle

4. Experimental procedures

4.1. Manufacturing of an ABS printed specimens

The optimised MBB beam STL file format of the optimised MBB beam have been exported from ABAQUS and converted to the G-code file in order to be read by the FFF machine. It has been additively fabricated through Inder 3 S1 3D printer using an acrylonitrile butane styrene (ABS) material and polyvinyl alcohol (PVA) soluble support, as it is seen in Figure 6.

Fig. 6. Optimised structure manufactured with ABS material and PVA support

The optimised MBB beam was printed according to three raster angles, transverse at 90°, inclined at 45° and axial direction at 0°, as shown in Figure 7. Five specimens were printed at each raster angle. The total of the specimens tested is 5 x 3 = 15 samples for testing. The specimens were printed with the identical print settings of the digital models. Table 2 displays the measurements of the total mass of all printed samples obtained through an analytical balance.

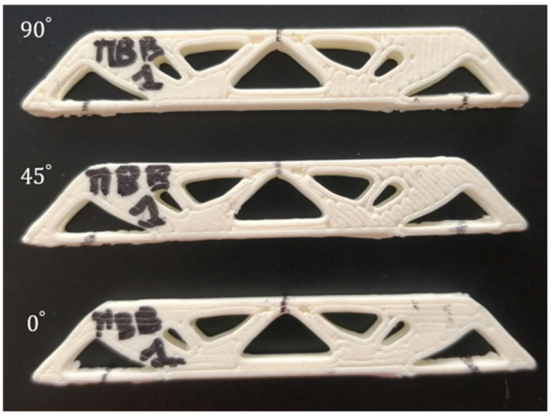

Fig. 7. Three raster angles used for the test

Table 2.
Mass of printed optimised structures

Raster angle	90°	45°	0°
Mass, g	1.3387±0.1	1.3605±0.1	1.3572±0.1

4.2. Three-point bending test

The specimens are three-point bending tested using an MTS 810 machine with a maximum load of 100 KN, as shown in Figure 8. The bending test is performed using a vertical displacement of 0.03 mm/sec, the distance between the spans is 50 mm, and the load-displacement curves have been recorded.

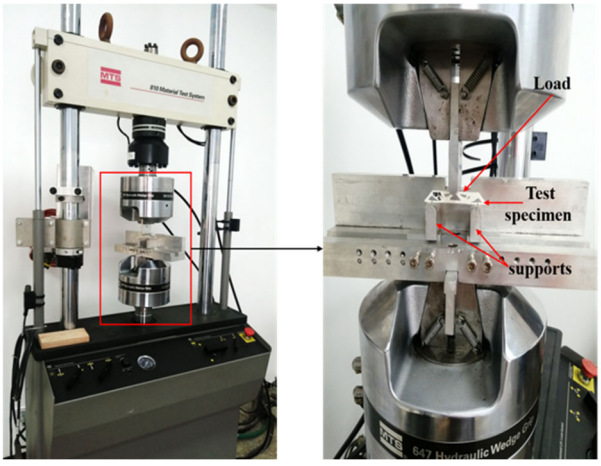

Fig. 8. Three-point bending test set up of the optimised MBB beam using MTS 810 machine

The bending test was chosen to study the mechanical behaviour of the optimised printed structures through the determination of the flexural stress and strain that were calculated as follows [16]:

$$\sigma_f = \frac{3FL}{2bd^2} \tag{3}$$

$$\varepsilon_f = \frac{6Dd}{L^2} \tag{4}$$

where F is the maximum load (N), L is the length of the support span (mm), and b and d are the width and depth of the sample (mm). D is the maximum deflection of the centre of the sample (mm).

5. Results and discussion

5.1. Numerical results

Figure 9 illustrates the von Mises stress distribution on the three digitals structures. The stress is highly concentrated in the digital models of 45° and 0° raster angle, and it is concentrated at the top as expected.

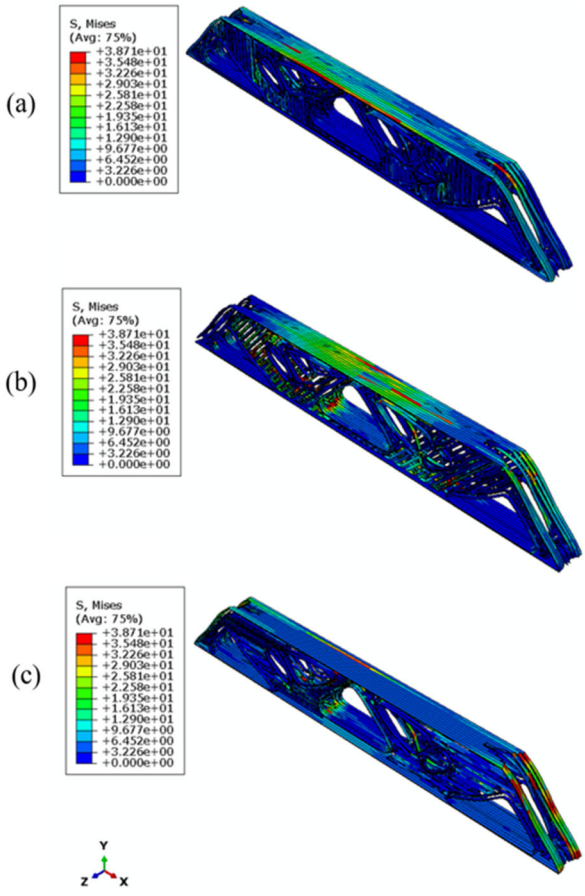

Fig. 9. Von Mises Stress distribution for (a) 90°, (b) 45° and (c) 0°

The stress distribution is also concentrated in the struts of the central interface on the digital structures of 45° and 0° where the failure has been predicted for the physical specimens and hardly any constraints at 90°, as illustrated in Figure 10 indicating that the virtual. model of 90° has better performance than 45° and 0° raster angle.

5.2. Experimental results

In order to depict the behaviour of the MBB beams printed with different raster angles, load-displacement curves of specimens are compared for an imposed displacement of 6 mm. In this study, the representative curves displayed in Figure 11. are determined by averaging the five curves for each sample type. The load-displacement curves of all three studied specimens show an initial linear phase. At the end of this linear phase, the load-displacement curves exhibit a non-linear convergence to the yield point and then material failure.

Furthermore, the maximum load supported by beams of 90°, 45° and 0° is 1778.38, 1571.40 and 1489.80 N, respectively, and their deflections at maximum load are 4.99, 3.71 and 3.67 mm respectively. Regarding the mechanical properties, the 0° angle raster has the weakest performance, with flexural stress of 65.62 MPa, otherwise, the specimen printed with a 90° raster angle has the highest performance, with a flexural stress of 79.86 MPa. For the 45° raster angle, the specimen also has the weakest performance compared to the 90° raster angle. Table 3. summarises the flexural properties of the specimens according to the three raster angles used.

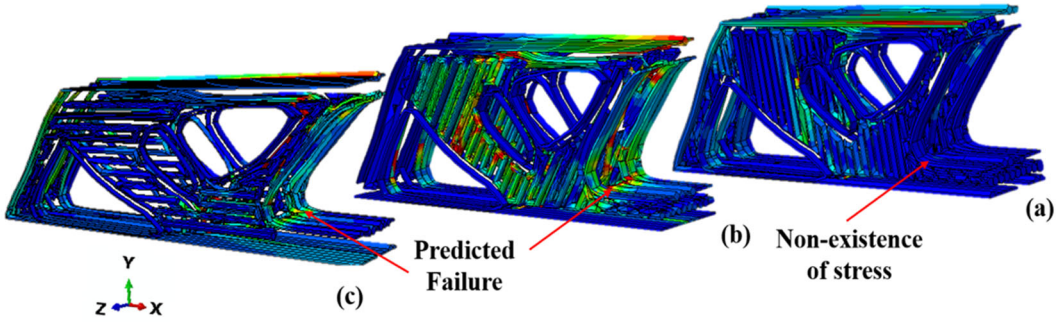

Fig. 10. Cross-section of half the optimised beams for (a) 90°, (b) 45° and (c) 0°

Table 3.
Flexural properties of the specimens

Samples	Load, KN	Flexural stress, MPa	Flexural strain, %
90° raster angle	0.17	79.86	4.7
45° raster angle	0.15	70.31	3.56
0° raster angle	0.14	65.62	3.52

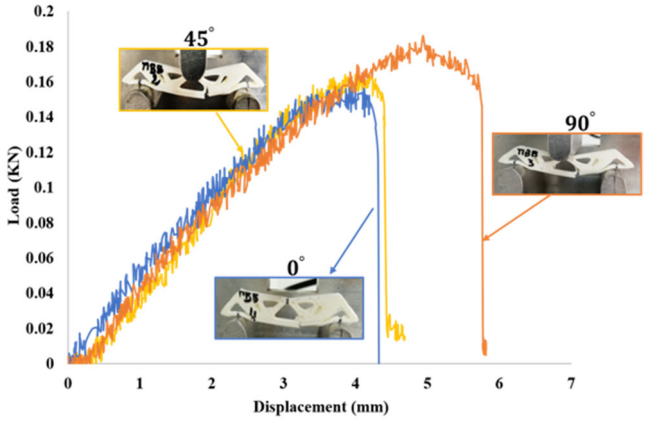

Fig. 11. Load-displacement curves for three-point bending test on the optimised specimens

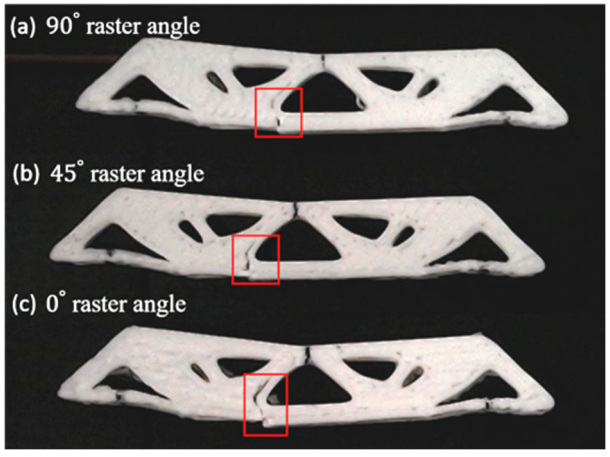

Fig. 12. Three raster angles fracture

Finally, Figure 12 illustrates representative structures after the bending test. The highlighted regions in the red present the failure zones. All specimens had deformations in the support areas and failed at the interface on one of the inclined struts, as the numerical results predicted. Note that the failure of the specimen fabricated by 0° raster angle has been propagated along the central interface than the other angles.

5.3. Discussion of the results

According to the experimental findings, it is obvious that the choice of raster angle has a meaningful effect on the mechanical behaviour of the optimised ABS printed structures. In particular, the calculated bending stress and strain of all samples showed that the specimen printed with a 90° raster angle exhibited better performance and followed by the specimen printed with 45°, and for specimen printed with 0° presented the weakest performance. In other words, the filament parallel to the applied load has a better mechanical performance than the orthogonal filament. When the filament is oriented in the direction of the load, the optimised structure will be stiffer (45° case). Moreover, the force required to shatter the overlay is greater than that required to shatter the filament; the explanation for why the sample printed with 90° is stiffer than the 0°, where the overlap is at the top and in front with the applied load unlike the sample printed by 0°, that was disrupted by means of a to the separation of the layers. For the numerical data, the von Mises stress distribution in the virtual structure of 90° is lower than the 45° and 0°. Whereas the von Mises stresses in the virtual structure of 45° are more highly concentrated than 0°.

In order to verify our numerical approach, a comparative study was performed with the experimental results of load-displacement curves for each type of geometry and reported in Figure 13. The numerical results agree with the experimental tests in the linear elastic regime of all the samples. The numerical data and the experimental test were compared for the ultimate load presented in Figure 14. Table 4 displays the error at ultimate load for numerical and experimental results calculated in the plastic region where the divergence existed.

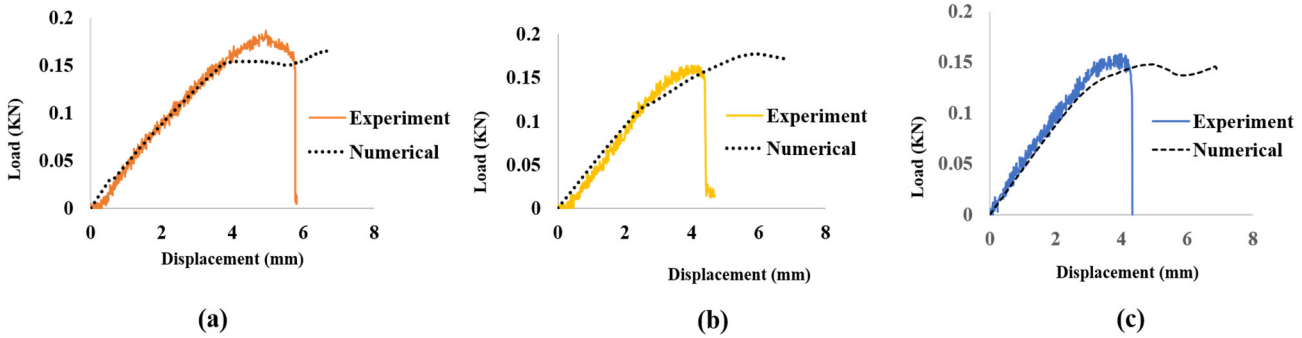

Fig. 13. Experimental and numerical comparison of load-displacement raster angle for (a) 90°, (b) 45° and (c) 0°

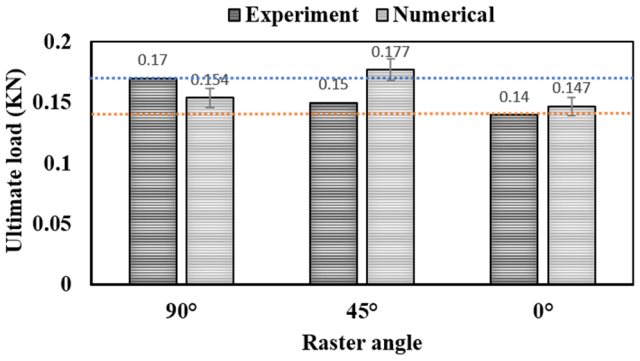

Fig. 14. Experimental and numerical comparison of ultimate load for each raster angle

Table 4.
The error between numerical and experimental results (RMSE method)

Raster angle	90°	45°	0°
Error, %	0.73	1.9	0.64

However, the discrepancies in the plastic regions of the experimental and numerical curves are correlated to the non-isotropy of the material, which is assumed to be isotropic in numerical simulation or the slippage of the samples across the span of the bending test support given the glossy surface which induces inaccuracies in the experimental results.

6. Conclusions

This research presents a novel numerical approach to investigate the effect of raster angle on the mechanical behaviour of structures optimised topologically according to the SIMP method and printed in ABS. The optimised structures were subject to the three-point bending test. From the numerical data, the distribution of the von Mises stress in the virtual structure of 90° raster than the virtual structures of 45° and 0°. The experimental results of the optimised structures printed in ABS show that the optimised structure printed with a 90° raster angle has better mechanical performance, followed by 45° and 0°. A comparison between the numerical data and experimental results was performed to verify the potential of the proposed approach, and the error is about 1.09%.

In contrast, the current researchers have found an error higher than 2%. The numerical data corroborate the experimental results perfectly. Therefore, our numerical approach allows to simulate optimised printed structures considering the FFF manufacturing parameters.

Future work will be devoted to developing the numerical approach to incorporate the anisotropy properties and decrease the computing time.

References

[1] M.P. Bendsøe, O. Sigmund, Topology: theory, methods, and applications, Springer, Berlin, Heidelberg, 2013. DOI: https://doi.org/10.1007/978-3-662-05086-6

[2] M.P. Bendsoe, N. Kikuchi, Generating optimal topologies in structural design using a homogenization method, Computer Methods in Applied Mechanics and Engineering 71/2 (1988) 197-224. DOI: https://doi.org/10.1016/0045-7825(88)90086-2

[3] K. Suzuki, N. Kikuchi, A Homogenization Method for Shape and Topology Optimization, Computer Methods in Applied Mechanics and Engineering 93/3 (1991) 291-318. DOI: https://doi.org/10.1016/0045-7825(91)90245-2

[4] E. Abdeddine, A. Majid, Z. Beidouri, Kh. Zarbane, Experimental investigation for non-linear vibrations of free supported and cantilever FFF rectangular plates, Archives of Materials Science and Engineering 116/2 (2022) 49-56. DOI: https://doi.org/10.5604/01.3001.0016.1189

[5] A.E. Costa, A. Ferreira da Silva, O. Sousa Carneiro, A study on extruded filament bonding in fused filament fabrication, Rapid Prototyping Journal 25/3 (2019) 555-565. DOI: https://doi.org/10.1108/RPJ-03-2018-0062

[6] A.W. Gebisa, H.G. Lemu, Influence of 3D printing FDM process parameters on tensile property of ULTEM 9085, Procedia Manufacturing 30 (2019) 331-338. DOI: https://doi.org/10.1016/j.promfg.2019.02.047

[7] V. Kandemir, O. Dogan, U. Yaman, Topology optimization of 2.5 D parts using the SIMP method with a variable thickness approach, Procedia Manufacturing 17 (2018) 29-36. DOI: https://doi.org/10.1016/j.promfg.2018.10.009

[8] A.A. Garcia-Granada, J. Catafal-Pedragosa, H.G. Lemu, Topology optimization through stiffness/weight ratio analysis for a three-point bending test of additive manufactured parts, IOP Conference Series: Materials Science and Engineering 700/1 (2019) 012012. DOI: https://doi.org/10.1088/1757-899X/700/1/012012

[9] S.R. Mohan, S. Simhambhatla, Adopting feature resolution and material distribution constraints into topology optimisationof additive manufacturing

components, Virtual and Physical Prototyping 14/1 (2019) 79-91.
DOI: https://doi.org/10.1080/17452759.2018.1501275
[10] N.S. Hmeidat, B. Brown, X. Jia, N. Vermaak, B. Compton, Effects of infill patterns on the strength and stiffness of 3D printed topologically optimized geometries, Rapid Prototyping Journal 27/8 (2021) 1467-1479.
DOI: https://doi.org/10.1108/RPJ-11-2019-0290
[11] Rashid, R., Masood, S. H., Ruan, D., Palanisamy, S., Huang, X., and Rahman Rashid, R. A. Topology optimisation of additively manufactured lattice beams for three-point bending test, Proceedings of the 29th Annual International Solid Freeform Fabrication Symposium – An Additive Manufacturing Conference, University of Texas, Austin, 2018, 635-645. DOI: http://dx.doi.org/10.26153/tsw/17066
[12] O. Sigmund, K. Maute, Topology optimization approaches, Structural and Multidisciplinary Optimization 48/6 (2013) 1031-1055. DOI: https://doi.org/10.1007/s00158-013-0978-6
[13] O. Sigmund, A 99 line topology optimization code written in matlab, Structural and Multidisciplinary Optimization 21/2 (2001) 120-127.
DOI: https://doi.org/10.1007/s001580050176
[14] M. Othmani, K. Zarbane, A. Chouaf, Enhanced mesostructural modeling and prediction of the mechanical behavior of acrylonitrile butadiene styrene parts manufactured by fused deposition modeling, International Review of Mechanical Engineering 14/4 (2020) 243-252.
DOI: https://doi.org/10.15866/ireme.v14i4.17736
[15] I. Antar, M. Othmani, Kh. Zarbane, M. El Oumami, Z. Beidouri, Topology optimization of a 3D part virtually printed by FDM, Journal of Achievements in Materials and Manufacturing Engineering 112/1 (2022) 25-32. DOI: https://doi.org/10.5604/01.3001.0016.0289
[16] ISO 178:2019 - Plastics — Determination of flexural properties, ISO, 2003.